Surface-Enhanced Raman Scattering from Metallic Nanostructures: Bridging the Gap between the Near-Field and Far-Field Responses

Doherty, M. D., Pollard, R. J., Dawson, P., & Murphy, A. (2013). Surface-Enhanced Raman Scattering from Metallic Nanostructures: Bridging the Gap between the Near-Field and Far-Field Responses. Physical review x, 3(1), [011001]. DOI: 10.1103/PhysRevX.3.011001

Published in:
Physical review x

Document Version:
Publisher's PDF, also known as Version of record

Surface-Enhanced Raman Scattering from Metallic Nanostructures: Bridging the Gap between the Near-Field and Far-Field Responses

Matthew D. Doherty,* Antony Murphy, Robert J. Pollard, and Paul Dawson

Centre for Nanostructured Media, School of Mathematics and Physics, Queen's University Belfast, Belfast BT7 1NN, United Kingdom

(Received 23 August 2012; published 10 January 2013)

We present here a detailed study of the complex relationship between the electromagnetic near-field and far-field responses of "real" nanostructured metallic surfaces. The near-field and far-field responses are specified in terms of (spectra of) the surface-enhanced Raman-scattering enhancement factor (SERS EF) and optical extinction, respectively. First, it is shown that gold nanorod- and nanotube-array substrates exhibit three distinct localized surface plasmon resonances (LSPRs): a longitudinal, a transverse, and a cavity mode. The cavity mode simultaneously has the largest impact on the near-field behavior (as observed through the SERS EF) and the weakest optical interaction: It has a "near-field-type" character. The transverse and longitudinal modes have a significant impact on the far-field behavior but very little impact on SERS: They have a "far-field-type" character. We confirm the presence of the cavity mode using a combination of SERS EF spectra, electron microscopy, and electromagnetic modeling and thus clearly illustrate and explain the (lack of) correlation between the SERS EF spectra and the optical response in terms of the contrasting character of the three LSPRs. In doing so, we experimentally demonstrate that, for a surface that supports multiple LSPRs, the near-field and far-field properties can in fact be tuned almost independently. It is further demonstrated that small changes in geometrical parameters that tune the spectral location of the LPSRs can also drastically influence the character of these modes, resulting in certain unusual behavior, such as the far-field resonance redshift as the near-field resonance blueshifts.

DOI: 10.1103/PhysRevX.3.011001 Subject Areas: Nanophysics, Optics

I. INTRODUCTION

Noble metals that are structured on the nanoscale have attracted widespread interest over the past decade, principally due to their ability to support surface plasmon polaritons. Of particular interest here are localized surface plasmon-polariton resonances (LSPRs) supported by discrete (but interacting) metallic nanostructures. Two key characteristics are associated with the excitation of LSPRs: strong wavelength-selective (and often polarization-selective) optical extinction in the far field and highly enhanced local electromagnetic fields in the near field [1,2]. Much of the usefulness of metallic nanostructures is derived from the fact that their LSPRs can be finely controlled by changing their size, shape, or composition or the dielectric properties of their surroundings, effectively allowing for the control of light on the nanoscale [3–5]. The subdiffraction-limit focusing of electromagnetic fields in the near field on LSPR excitation is responsible for the huge signal increases observed in surface-enhanced spectroscopies and, of specific interest here, those observed in surface-enhanced Raman scattering (SERS) [6,7]. While a general understanding of the mechanism of SERS has long been established (albeit not without some controversy surrounding single-molecule SERS), there still remain some significant gaps in the detailed understanding of the interplay between near-field "hotspot"-driven SERS activity, the far-field optical response, and system geometry. In particular, these gaps concern the commonly held assumption that SERS is best performed in a spectral region where there is an obvious optical feature due to an LSPR. Not so—or, at least, not necessarily so—especially in the context of large-area nanostructured substrates of real applicability potential, as opposed to individual antenna structures that have been carefully crafted (by *e* beam, etc.). In this article, we first explain the issues in more detail in the following paragraphs and then address the intricate relationship between the optical near field (as measured using SERS) and far field (as observed in transmission or reflection measurements) in a quantitative and radical manner, with reference to both experimental and theoretical results from LSPRs supported by gold nanorod and gold nanotube arrays [8–10].

In SERS, the Raman cross section of absorbed molecules is massively increased, first due to the enhanced local fields exciting the Raman dipole and then—as a result of optical reciprocity—due to the enhancement of the instantaneous reemission of radiation by the dipole. The nonlinear relationship between the enhancement factor (EF) and the local electromagnetic-field strength is given approximately by the well-known equation

*mdoherty48@qub.ac.uk

$$\mathrm{EF} = \frac{|E_{\mathrm{loc}}(\omega_{\mathrm{I}})|^2 |E_{\mathrm{loc}}(\omega_{\mathrm{R}})|^2}{|E_{\mathrm{inc}}|^4}, \quad (1)$$

where E_{loc} is the local field at a point in the geometry, E_{inc} is the incident field strength, and ω_{I} and ω_{R} are the incident and Raman-scattered frequencies [11]. SERS substrates typically exhibit average EFs of 10^5–10^6, with EFs for individual analyte molecules under ideal conditions exceeding 10^{11} [6,12], allowing for observation of the Raman signal from single molecules in some situations [13,14]. Signal enhancements of this size have obvious potential for application in biological and chemical sensing, as signal levels in conventional Raman spectroscopy are often very low. In order to exploit this potential, much research has been undertaken into the fabrication of SERS substrates for routine analysis with a large average EF that are uniform, reproducible, and can be tailored for a particular excitation wavelength [15–17].

The ability to maximize the EF for a specific excitation wavelength is of particular interest, as typical Raman spectroscopy systems often have only one excitation source. Unfortunately, measurement of the SERS EF of a substrate across a wide spectral range is experimentally demanding, and therefore the optical signatures of LPSRs observed in transmission or reflection experiments are often used as a more convenient guide to the wavelengths at which a SERS substrate might be most effective. As mentioned above, the presence of a strong optical resonance is often taken as direct evidence of a wavelength with a favorable SERS EF, and, for some specific substrates, a direct link between optics and a SERS EF has indeed been experimentally demonstrated [18,19]. This connection is reasonable, in principle, as at resonance the interaction of the surface with the external field is maximized and therefore local fields generated by the LSPR—and hence by the SERS EF—should be maximized. In other words, the LSPRs supported by a surface are responsible for both the optical response and the SERS behavior, and therefore it seems reasonable that they should correlate with each other. However, for complex surfaces where multiple collective LSPRs are present—as is often the case for large-area ''bottom-up''-fabricated SERS substrates and colloid-based solutions of SERS-active metal particles—the link between conventional optical characterization and SERS EFs can become much more indirect [20]. This fact has been demonstrated previously in certain contexts: For example, it has been demonstrated that in colloidal systems there is little correlation between SERS and optical response [21–23] and more generally that areas of very large electric fields (so-called hotspots) in the near field of colloidal clusters and rough surfaces are highly dependent on the fine details of the geometry and do not correlate well with the far field [24,25]. The explanation for this breakdown lies in the differing origins of the optical and SERS properties of a surface, as provided in Ref. [20]: Optical properties such as extinction are determined entirely by the far-field behavior of a plasmonic substrate (scattering, reflection, etc.), whereas SERS is a near-field phenomenon that is generally maximized [according to Eq. (1)] when the electric fields are as localized as possible. Different LSPRs exhibited by a metal surface can be arbitrarily classified as having a more ''far-field-type'' or ''near-field-type'' character, according to how strongly they interact with incident radiation and how well they localize or focus electric fields. A far-field-type LSPR interacts strongly with the incident field without having any highly focused areas of intense electromagnetic field and therefore exhibits a large absorption or scattering cross section without providing any significant SERS enhancement. The opposite is true of a near-field-type LSPR that can have a small optical signature while generating a few areas of highly focused local fields at the surface—hotspots—that then provide a large SERS EF [20]. It has been demonstrated previously that extremely small numbers of molecules absorbed in these hotspots (usually a sharp edge or narrow gap) will often generate the majority of the observed Raman signal [26]. The occurrence of these two types of resonance on the same surface can translate into a lack of correlation between SERS and optical response: One LSPR can dominate the optical signature of a surface while having a negligible effect on the SERS performance and vice versa. As a result of the existence of multiple resonances of contrasting character, even relatively simple systems—such as the canonical metallic dimer with a nanometer-scale gap—can display a poor correlation between near and far fields, as the far-field properties are dominated by the interaction with the dipolar LSPR, while the near fields in the gap responsible for SERS have a multipolar character [27,28].

The work presented here has utilized a combination of wavelength-scanned SERS, conventional optical measurements, electron microscopy, and numerical modeling to probe in detail the often complex relationship between the near-field (SERS) and far-field (optical) properties of a plasmonic surface supporting multiple collective LSPRs. Indeed, we properly specify and demonstrate in a comprehensive manner for the first time the various regimes of near-field and far-field interplay. To achieve this demonstration, we have used a range of gold nanorod- and nanotube-array substrates [8–10] exhibiting three distinct LSPRs: These are classified as longitudinal-, transverse-, and cavity-mode LSPRs on the basis of their overall field distributions. The far-field properties of these modes have been demonstrated previously [8,9,29,30], but here we utilize precise control over the geometrical parameters of the structures to demonstrate in unprecedented experimental and theoretical detail how the differing character of these modes affects the far field, the near field, and the relationship between these two sets of properties on any given surface. In addition, by utilizing this fine control over fabrication parameters, we have also investigated

the crucial importance of geometry in determining not only the spectral location but also the character of the LSPRs and have demonstrated both experimentally and with computational models that small structural changes can change the behavior of a resonance from far-field type to near-field type and vice versa. The relationship between the near- and far-field behavior of plasmonic substrates is of broad interest not only for SERS but also for other potential applications, such as solar cells [31] or extreme light concentration [5].

II. THE FAR FIELD

Quasiordered nanorod arrays are prepared by electrodeposition of gold into porous anodized alumina templates grown on glass substrates, as described elsewhere [8]. Au nanotube arrays are prepared using a similar technique, where polypyrrole is initially deposited into the alumina templates and Au is subsequently electrodeposited into a hollow shell etched around the polypyrrole core [9]. The geometrical parameters of the alumina template are used to control the array period and nanorod or nanotube spacing; the polypyrrole core and subsequent shell etches are used to control the core size and wall thickness of the nanotubes, respectively; and the length of the nanorods and nanotubes is controlled by varying the length of the electrodeposition stage [8,9]. After electrodeposition, the alumina template and polypyrrole cores are removed via plasma and chemical etching, leaving a freestanding array of Au nanostructures. [The case of nanorods is shown in Figs. 1(a) and 1(b).]

Optical-transmission spectroscopy and electromagnetic modeling of Au nanorod arrays reveal pronounced peaks in extinction in the visible range [Fig. 1(c)] due to transverse (green spectrum) and longitudinal (red spectrum) LSPRs. Figure 1(c) shows two modeled spectra, used here to typify the far-field response; they closely resemble experimental spectra, with the exception that the experimental spectra can show a rising background toward the red (see Fig. 2) due to a thin Au underlayer used as a counterelectrode during the electrodeposition process. The transverse and longitudinal LSPRs are similar in nature to those of isolated gold nanorods and are excited by incident light polarized along the short and long axes of the nanorods, respectively, and the energy (or wavelength) of the resonances is determined by the aspect ratio [6,32,33]. In the case of arrays of aligned nanorods, the energy of the LSPRs is additionally affected by the interaction with the LSPRs of the neighboring nanorods [34,35]: Coulombic

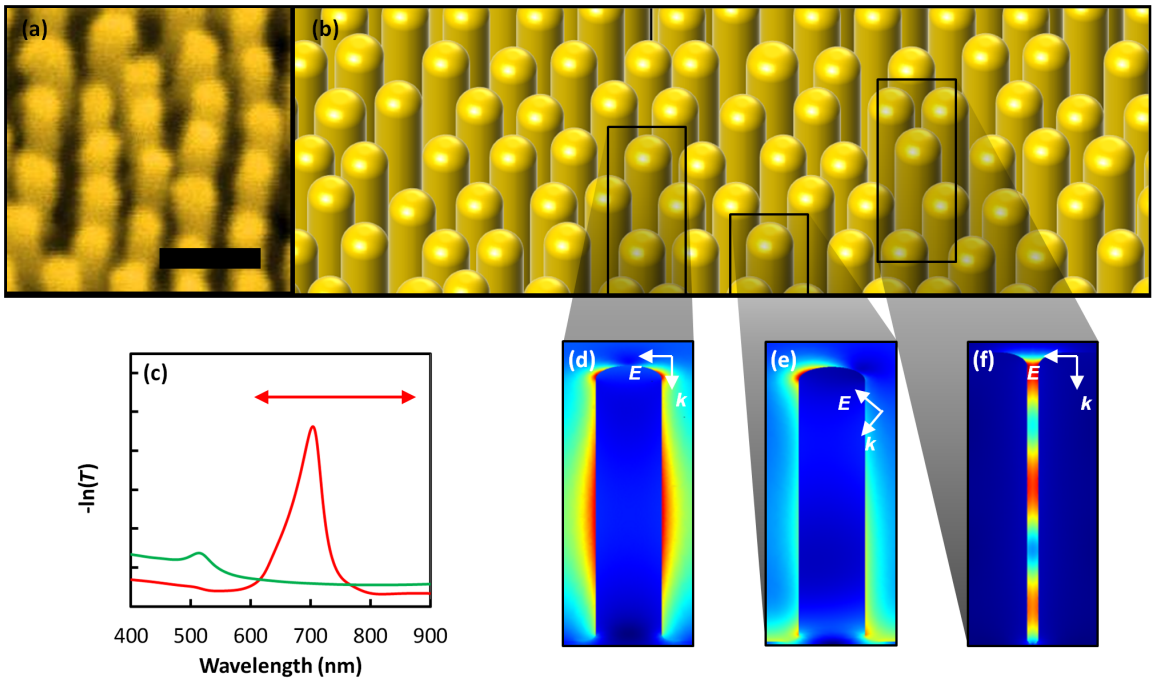

FIG. 1. Scanning electron microscope (SEM) image and schematic illustration of a quasiordered freestanding nanorod array, along with typical optical-extinction spectra [$-\ln(T)$] and near-field profiles on excitation of LSPRs. (a) SEM image taken at 40° from normal of Au nanorods (scale bar = 100 nm) and (b) matching schematic illustration. (c) Modeled extinction spectra of nanorod arrays in air: The green spectrum is for normal incidence excitation, showing the transverse LSPR of the nanorods. The red spectrum is for 40°-incidence excitation by *p*-polarized light and illustrates the longitudinal LPSR for 450-nm-long nanorods. The red arrow indicates the range of tunability of the longitudinal LSPR. Plots of the modeled electromagnetic field in the near field of nanorods illustrate the excitation of the (d) transverse-, (e) longitudinal-, and (f) cavity-mode LSPRs. In (d) and (e), the inter-rod gap is 40 nm, while in (f) it is 4 nm. In (d)–(f), the array period is 65 nm and the nanorods are 200 nm long. E and k as marked indicate the polarization and wave vector of the incident radiation, respectively.

repulsion between neighboring rods oscillating in phase causes the longitudinal resonance to significantly blueshift with respect to that of an isolated rod, and therefore, even for rods with very high aspect ratios, the longitudinal LSPR of the array can occur in the visible range. The blueshift of the longitudinal LSPR increases as inter-rod spacing decreases, and for very small spacing this mode can become fully degenerate with the transverse LSPR at 500–550 nm [35].

The wavelength-dependent response of the near field of the nanorod arrays to linearly polarized light is simulated under periodic boundary conditions with a hexagonal unit cell using the finite-element method of numerical analysis. Characteristic near-field radiation patterns on excitation of the transverse and longitudinal resonances are shown in Figs. 1(d) and 1(e), respectively: For the transverse LSPR, electric-field intensity is concentrated between the nanorods, and, on excitation of the longitudinal resonance, fields are focused at the top and bottom of the structures. Computational modeling also reveals a third resonance, appearing only when the inter-rod gap is narrow: a cavity resonance, shown in Fig. 1(f). Importantly, however, it leaves no observable optical signature or, in other words, it is not observed experimentally in the far-field optical response of our substrates. This resonance appears superficially similar to the longitudinal LSPR in that it is dependent on the height of the nanorods, but it is in fact an independent mode and fundamentally different in nature. When the inter-rod gap is sufficiently small, the transverse LSPRs of neighboring nanorods become highly coupled and the structure begins to behave similarly to a metal-dielectric-metal waveguide. Plasmonic metal-dielectric-metal modes traveling along the gap between neighboring nanorods are excited by light at normal incidence and reflected by the gold underlayer with a π-phase shift, forming a plasmonic standing wave, or cavity resonance, with a node at the metal end and an antinode at the open end [29,30]. External illumination is most efficiently coupled into the cavity mode on excitation of quarter-wave resonances; the wavelength of these resonances is proportional to $2h/(2i+1)\pi$, where i determines the order of the harmonic [excitation of the fifth harmonic is shown in Fig. 1(f)] and h is the height of the cavity. As a result, the cavity resonances are redshifted as the length of the nanorods increases [29]. The cavity mode is polarized in the plane of the array, and therefore Coulombic attraction between neighboring rods causes the resonance to redshift with decreasing gap width, behavior that is opposite to that of the longitudinal LSPR [35]. Modeling of the cavity LSPR for perfectly periodic arrays predicts maxima of transmission or minima of reflection at resonance (again in contrast to the longitudinal LSPR), and this behavior has previously been observed experimentally for very well-ordered arrays [29]. However, as already noted, the cavity-mode LSPR is not observed optically on the substrates examined here. We believe that the quasiordered nature and the range of inter-rod gaps of these substrates are responsible for the lack of a visible optical signature of the cavity resonance for two key reasons: First, only a small fraction of the inter-rod gaps are sufficiently narrow to support this type of resonance. Second, for those gaps that are narrow enough, the resonance is broadened due to the strong dependence of the resonance wavelength on the inter-rod gap [29]. Similar effects have previously been demonstrated: It was shown for similar substrates that, as the disorder of the array increases, the optical signature of the cavity resonances is broadened and diminished [29]. Even though this resonance does not have a strong optical presence on these substrates, it plays a pivotal role in determining the SERS behavior of the substrates, as we demonstrate in Sec. III B.

III. THE NEAR-FIELD SERS

A. Transverse and longitudinal LSPRs

Raman spectra are recorded using a custom-built, open-bench Raman system in the backscattering configuration with seven different excitation lasers at wavelengths 532, 543, 594, 633, 671, 690, and 780 nm. (The details of the Raman spectroscopy technique are described elsewhere [36].) We use two probe molecules [crystal violet (CV) and rhodamine 6G (R6G)], aqueous solutions of which are applied to the surface using a micropipette and allowed to air dry, leaving a layer of adsorbed probe molecules on the gold surface. The concentrations of the solutions used (on the order of 1 μM) are chosen to give an approximately monolayer coverage of the nanostructured Au surface. Since we are interested in observing variations in the Raman intensity that are due only to the intrinsic spectral dependence of the SERS EF (and hence in studying the wavelength-dependent behavior of the near field), it is necessary to correct for variations in intensity due to differences in laser-illumination power, the inherent wavelength dependence of the Raman cross section of the molecules, chemical interactions between the molecule and the surface, and the overall detection efficiency of the system. To this end, the Raman band intensities obtained from these molecules are normalized against unenhanced spectra taken under the same experimental conditions from molecules held in solution in quartz cuvettes. We calculate the average EF, denoted as $\langle \mathrm{EF} \rangle$, using the rigorously defined "total SERS substrate EF" [12], which is expressed completely in terms of quantities measured by direct experiment as

$$\langle \mathrm{EF} \rangle = \frac{I_{\mathrm{SERS}}/\mu_{\mathrm{surf}}}{I_{\mathrm{RS}}/(c_{\mathrm{RS}} H_{\mathrm{eff}})}, \tag{2}$$

where μ_{surf} is the density of molecules on the surface, c_{RS} is the concentration of molecules in the absence of the metallic surface, H_{eff} is the effective height of the

scattering volume of the system, and I_{RS} and I_{SERS} are the corresponding reference Raman-scattering and SERS intensities. H_{eff} is calculated by carefully characterizing the scattering volume of the system using the 520-cm^{-1} phonon mode of silicon, employing methods similar to those described by Le Ru *et al.* [12]. The 775-cm^{-1} band of R6G and the 915-cm^{-1} band of CV are used to measure the *average* enhancement factor ⟨EF⟩, as they are intense, well separated from nearby Raman bands, and scatter at a very similar absolute wavelength. For this situation, the electromagnetic SERS EF for each molecule should be very similar since it is dependent on the field enhancement at the excitation and scattered wavelengths, and therefore any significant chemical-enhancement or resonance Raman effects should be made obvious by a divergence of the EF measured for the two probe molecules.

Figure 2(a) plots the typical SERS response of a nanorod substrate where only the transverse LSPR at approximately 520 nm is visible optically (as well as a broad background rising into the red that is caused by the Au underlayer), while Fig. 2(b) shows the response of a nanorod substrate

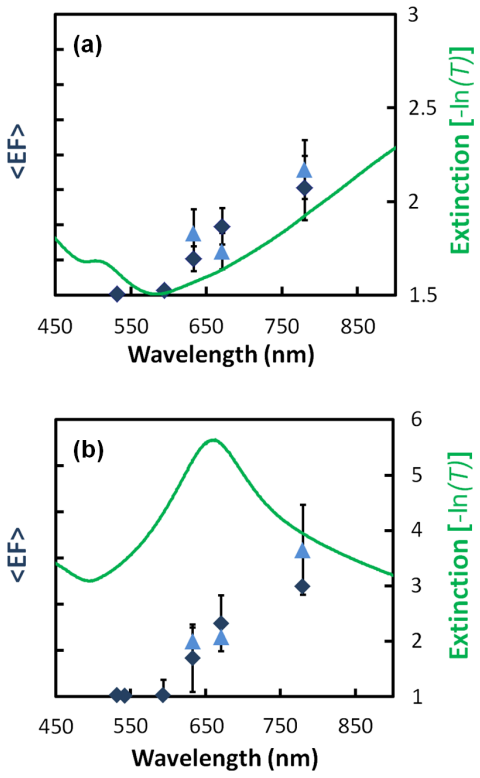

FIG. 2. Graphs comparing the observed SERS enhancement factor ⟨EF⟩ and optical extinction $[-\ln(T)]$ for the case of (a) 120-nm-long nanorods with average diameter 48 nm at 0° incidence and (b) 350-nm-long nanorods with average diameter 38 nm at 40° incidence (in both cases in the array, the period is 65 nm). The green lines indicate the optical extinction. Black-diamond and blue-triangle data points indicate the ⟨EF⟩ of the 915-cm^{-1} band of CV and the 775-cm^{-1} band of R6G, respectively. The scale on the ⟨EF⟩ axis is the same on both graphs. Enhancement factors are plotted at the excitation wavelength.

with a prominent longitudinal LSPR (approximately 650 nm). In these figures, the absolute values of ⟨EF⟩ are not marked, as the error in determining these values is much larger than the error in determining the relative ⟨EF⟩, i.e., the difference in ⟨EF⟩ from one wavelength to another. This uncertainty is due to the difficulty of precisely measuring the number of probe molecules absorbed by the surface. Typical values of ⟨EF⟩ observed on these substrates are on the order of 10^3–10^4, which is a significant enhancement, although they are on the lower end of values typically reported in the literature [37–39]. From these graphs, it is clear that neither the longitudinal nor the transverse LSPRs correlate well with the SERS EF. In Fig. 2(a), the optical transverse resonance has a peak at 520 nm but appears to be at its maximum in the far red at 780 nm. (The apparent correlation between the broad rising background and the SERS EF is purely coincidental, as that background is due to interaction with the gold underlayer, not a plasmonic resonance.) In Fig. 2(b), the optical resonance of the longitudinal LSPR peaks at 650 nm, while again the ⟨EF⟩ is at its maximum at 780 nm. That the transverse LSPR does not influence SERS enhancement is not surprising, as the near-field radiation patterns associated with this resonance lack focused areas of very high intensity with fields being spread along the long axis of the nanorods; i.e., the resonance has a more far-field-type character (see Fig. 1). In addition, this resonance occurs in the same spectral range as the Au interband transition, which acts to dampen the resonance and further reduce local field intensities. The longitudinal resonance, on the other hand, is not affected by these factors: As can be seen in Fig. 1(e), excitation of this resonance focuses electric fields well at the rod ends, and the resonance is typically in the red region of the spectrum away from the interband transition of Au, and therefore the lack of significant influence on the SERS is more surprising. In fact, the spectral dependence and magnitude of the EF appear remarkably similar in these two cases, despite the obvious differences in the optical signatures.

To further investigate why the longitudinal LSPR has so little impact on the SERS EF, we again utilize the finite-element method of computational near-field modeling. In order to facilitate direct comparison between modeling predictions and experimental results, we calculate the spatial average of the EF given by Eq. (1) (for an imaginary Raman band at 850 cm^{-1}), integrated over a 1-nm-thick layer covering the entire surface of the structure. This 1-nm-thick layer approximates a monolayer of analyte molecules covering the substrate surface, and thus the average EF ⟨EF⟩ calculated in this way is directly comparable to the experimentally observed value. Throughout this work, the terms average enhancement factor and ⟨EF⟩ are used to refer to data from either experiments or simulations as specified. As illustration, the average EF is modeled for the case of the longitudinal LSPR of an

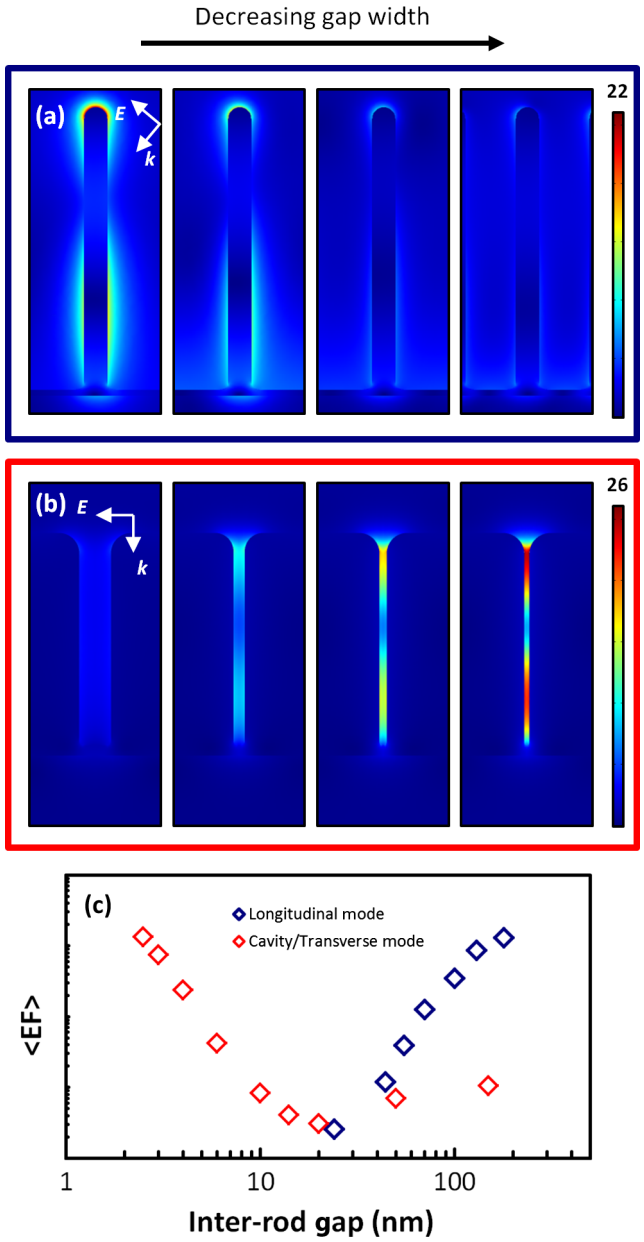

FIG. 3. Plots of the simulated local electromagnetic fields and enhancement factors around nanorod arrays as the inter-rod gap is decreased, showing the effect on the longitudinal and the transverse or cavity resonances. The nanorods shown in (a) are 250 nm long and 20 nm in diameter, with inter-rod gaps of 180, 100, 70, and 45 nm (at resonance wavelengths 960, 880, 800, and 650 nm, respectively). The nanorods shown in (b) are 100 nm long and 50 nm in diameter, with inter-rod gaps of 16, 6, 4, and 3 nm (at resonance wavelengths 540, 594, 633, and 671 nm, respectively). *E* and *k* as marked indicate the polarization and wave vector of the incident radiation. (c) shows a plot of the calculated average enhancement factor on resonance (on a logarithmic scale) as a function of the inter-rod gap for the rods shown in (a) and (b).

isolated nanorod 250 nm in length and 20 nm in diameter and for the same nanorods of the same dimensions in a hexagonal array with a range of periods. For the isolated nanorod, local electric fields of the longitudinal LSPR are focused very efficiently to the nanorod ends, giving a large average EF of 2.5×10^6. When the same nanorods are in an array, the optical signature of the longitudinal LSPR is similar, with the resonance wavelength blueshifting as the array period is decreased [35]. However, as the array period decreases, the local fields around the nanorods rapidly decrease, as illustrated in Fig. 3(a), and, for nanorods with an array period of 65 nm (typical of our substrates), the average SERS EF, at approximately 20, is staggeringly lower by 5 orders of magnitude. The observed $\langle EF \rangle$ of our substrates is on the order of 10^3–10^4, and therefore the longitudinal LSPR clearly cannot be responsible for the bulk of the SERS enhancement. This reduction in SERS enhancement has the same origin as the blueshift: the depolarizing effect of the Coulombic interactions between neighboring nanorods in the array [35]. As the array period decreases, the Coulombic repulsion increases between neighboring nanorods oscillating in phase, reducing the charge separation and hence the local fields and SERS EF. The dramatic magnitude of the EF decrease results from the nonlinear relationship between local fields and the EF [Eq. (1)]. The longitudinal resonance of gold nanorod arrays clearly illustrates how the near-field-type character of an LSPR can dramatically shift to far-field type as the resonance location is tuned. This is a crucially important point in general, as any method of tuning the spectral location of an LSPR—changing the geometry, interaction with neighboring structures, or interaction with the dielectric environment—is likely to affect the character of the resonance in some way, and therefore the tuning of far-field LSPRs may not correspond well to the near-field behavior and vice versa. This point is reinforced with experimental evidence in Sec. IV.

B. Cavity LSPR

In fact, on these substrates, the vast majority of the SERS enhancement is generated by the (optically insignificant) cavity resonance. Models similar to those above have been run for nanorods that are closely spaced so that the transverse LSPRs of neighboring nanorods strongly couple and behave as a cavity, and the average EF is again calculated. On excitation of the third harmonic of the cavity mode of a nanorod array with a 4-nm inter-rod gap, the average EF is 6×10^3, a significantly greater number than for the longitudinal LSPR. As the gap is decreased further, this number increases rapidly, as illustrated in Figs. 3(b) and 3(c) [36]. The contrast between the behavior of this mode and that of the longitudinal LSPR as the inter-rod gap is varied is illustrated in Fig. 3(c). Unlike the longitudinal LSPR, the cavity resonance cannot be excited anywhere on a typical substrate: It can only exist in very narrow inter-rod gaps (<10 nm). However, as a result of the large EF provided by this resonance, even for the case when less than 10% of the gaps present are narrow enough to support it (as is the case on a typical

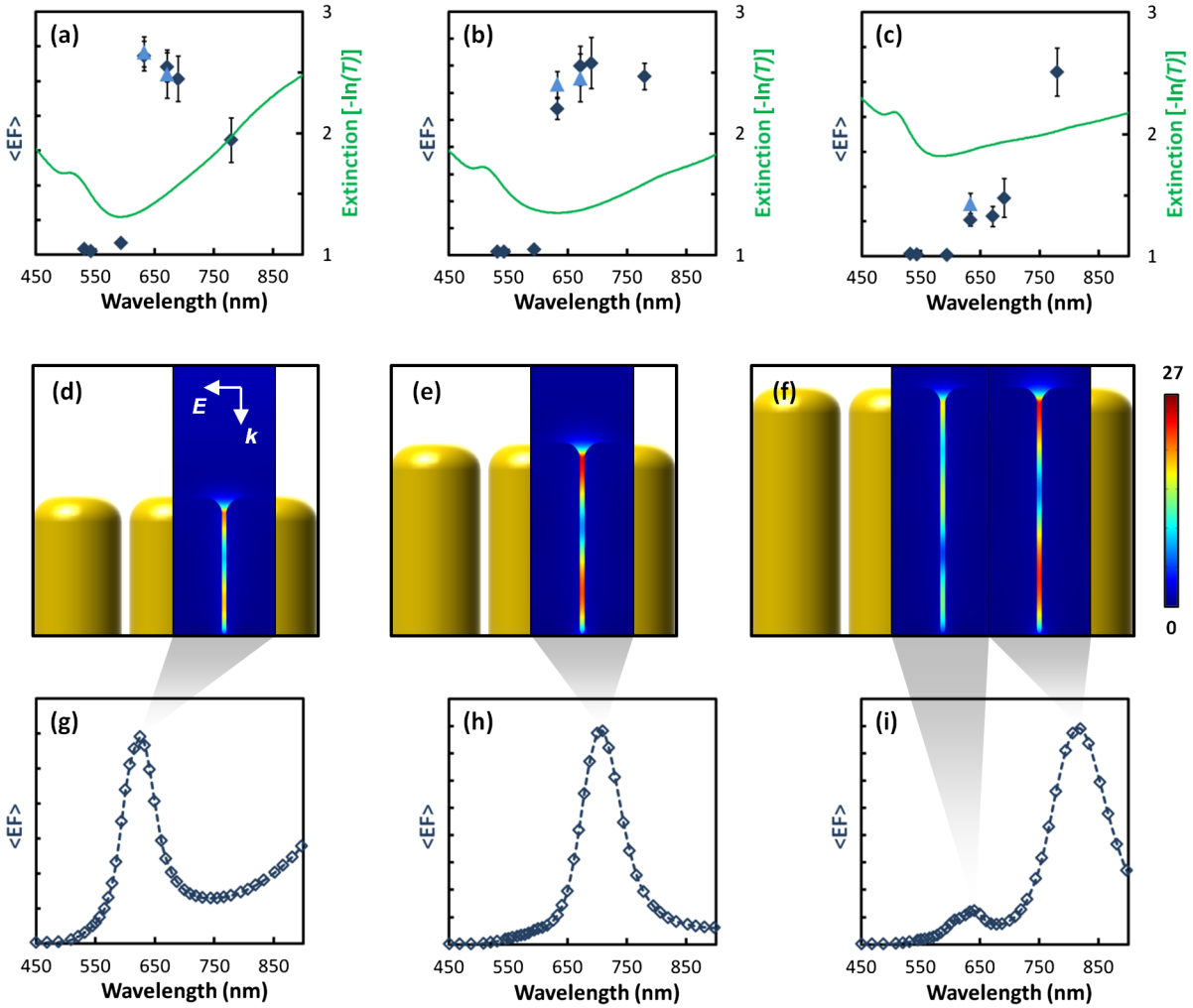

FIG. 4. Graphs of the observed and modeled enhancement factor, demonstrating the effect of the cavity mode on SERS. (a)–(c) Graphs comparing the measured enhancement factor ⟨EF⟩ and optical extinction [− ln(*T*)] at normal incidence for nanorods with an average diameter of 48 nm; array period of 64 nm; and average lengths of (a) 85, (b) 125, and (c) 160 nm. The green lines indicate the optical extinction. Black-diamond and blue-triangle data points indicate the ⟨EF⟩ of the 915-cm^{-1} band of CV and the 775-cm^{-1} band of R6G, respectively. (d)–(f) Schematics of the modeled nanorod structures with 3-nm separation; array period of 64 nm; and lengths of (d) 85, (e) 125, and (f) 160 nm, overlaid with plots of local field on excitation of the third harmonic of the cavity. The fifth harmonic is also shown in (f) for the longest nanorods. (g)–(i) Graphs displaying the EF predicted by the finite-element-method modeling for the nanorods shown in (d)–(f). The hollow diamond data points indicate the predicted enhancement factor for an imaginary 850-cm^{-1} Raman band. All enhancement factors are plotted at the excitation wavelength.

substrate), the SERS enhancement generated by the cavity resonance is still much larger than any other LSPR and therefore it dominates the SERS behavior of the substrate. Parenthetically, as has been shown previously, the cavity mode of a particular gap is largely unaffected by the lack of perfect order in the surrounding gaps [36]. The contrast between the behavior of the cavity and of longitudinal LSPRs clearly illustrates how unreliable the far-field optical response can be as a guide to SERS enhancement: For this system, a cavity resonance occurring at approximately 650 nm can be expected to provide up to 3 orders of magnitude more enhancement than a longitudinal resonance in the same spectral location, despite its weak optical signature.

As detailed above, the wavelength of the cavity resonance depends on the height of the nanorods; thus, to experimentally confirm the cavity mode's existence using SERS, we fabricate a set of nanorod-array substrates with small inter-rod gaps and varying rod lengths in the range of 50–200 nm. These geometrical parameters are chosen so that the longitudinal and transverse LSPRs are degenerate at approximately 520 nm, to ensure that these resonances will have little impact on the SERS. The ⟨EF⟩ spectra and optics of these substrates are shown in Figs. 4(a)–4(c). It is immediately clear that there is, as expected, no correlation between the SERS EF and the far-field optical response of the substrates. The optical signatures of the three substrates shown are very similar, with all three exhibiting a

transverse LSPR at approximately 520 nm and a background rising into the red due to the gold underlayer, whereas the ⟨EF⟩ or average EF of each substrate has a maximum EF at a different wavelength. The average inter-rod gap observed on these substrates is too wide to support a cavity mode, and therefore most nanorods exhibit the normal transverse LSPR. However, a small percentage of the gaps is sufficiently narrow, and, due to the very large EF generated by the cavity resonance, these gaps should dominate the SERS performance. For this reason, we choose to model arrays with a 3-nm gap. Figures 4(d)–4(i) show the modeled geometries and simulated ⟨EF⟩ for nanorod arrays of the same lengths as our samples, exhibiting a strong cavity resonance. It can be seen that, for the rod parameters chosen here, the third-order harmonic of the cavity redshifts across the visible range as the nanorod length increases from 85 to 160 nm. For the 160 nm nanorods, the fifth-order harmonic begins to appear. The fifth-order harmonic does not appear for the shorter nanorods, because, in these cases, it exists at a wavelength below 600 nm, where the interband transitions of gold heavily damp the resonance and suppress a strong interaction. The first-order harmonic of the cavity, on the other hand, is not seen here, because for these nanorods it occurs in the infrared range, well outside the modeled and experimentally observed wavelength range. On comparing spectra of the experimental ⟨EF⟩ and the modeled values of the EF, it is clear that there is a good correlation, confirming both the existence of the cavity resonance and that the third-order harmonic of the cavity is responsible for the bulk of the SERS enhancement observed in the visible range. However, the peaks of ⟨EF⟩ seen in the experimental results are much broader than those predicted by the modeling, which is likely due to the heterogeneous spacing between nanorods. As mentioned previously, and shown in Fig. 3, the cavity resonance is very sensitive to the inter-rod gap width, and therefore the distribution of gaps on these substrates will act to broaden the resonance. (Analysis of the substrate topography and distribution of inter-rod gaps is considered in more detail in [36].) The experimental values of ⟨EF⟩ in Fig. 4 are lower than the corresponding modeled ⟨EF⟩, as only a small percentage of the gaps present on the substrate surface support the cavity mode, whereas the model assumes a homogeneous narrow gap width. As an aside, if it were possible to fabricate substrates with very narrow (<5 nm) homogeneous inter-rod gaps, such substrates would be a very good candidate for a routine SERS substrate: They would present a high average EF, and tuning the spectral location of the maximum EF would be as simple as altering the length of the electrodeposition stage and hence the nanorod length.

Returning to the central theme, of the three LSPRs that we have identified in nanorod arrays, the cavity resonance is the only one that exhibits a near-field-type character. It focuses electromagnetic energy very efficiently into the narrow gap between rods, and therefore the impact on SERS is large, despite the fact that resonance does not interact strongly with the incident radiation (i.e., despite the lack of a strong optical signature). In contrast, the optical properties are dominated by the other two LSPRs present: the transverse and the longitudinal LSPRs. As a result of the existence of multiple LSPRs of contrasting character, there is a clear disconnect between the near-field and far-field behaviors of this surface. As can be seen in Fig. 2, the optical response can be tuned without significantly affecting the SERS response, and, in a contrary manner in Fig. 4, it is clear that the SERS behavior can be tuned almost independently of the optical properties.

IV. TUNING LSPRs—INFLUENCE ON THE NEAR FIELD AND FAR FIELD

In Sec. III A, we have described how "tuning" an LSPR from one wavelength to another can also profoundly affect the character of the resonance. In this section, the phenomenon is demonstrated experimentally. So far in the analysis, we have largely ignored the transverse resonance because for nanorods it has little impact on SERS, due both to its spectral location (in the absorbing interband region of gold) and to its far-field-type character. However, it is possible to alter both of these properties by using nanotubes, as illustrated in Fig. 5, instead of nanorods. At normal incidence, numerical modeling indicates that gold nanotube arrays exhibit the same fundamental LSPRs as nanorods, i.e., a transverse resonance for widely spaced nanotubes and a cavity resonance in the case of very closely spaced nanotubes. However, the resonances are altered in a number of crucial ways, as illustrated in Figs. 6(a)–6(c), where the scene is set, showing a schematic evolution from nanorods through thick-walled to thin-walled nanotubes. The cavity resonance is predicted to redshift with decreasing nanotube wall thickness (increasing the diameter-to-wall aspect ratio), and the local electric field associated with this resonance is considerably damped, massively reducing the SERS EF [as illustrated in

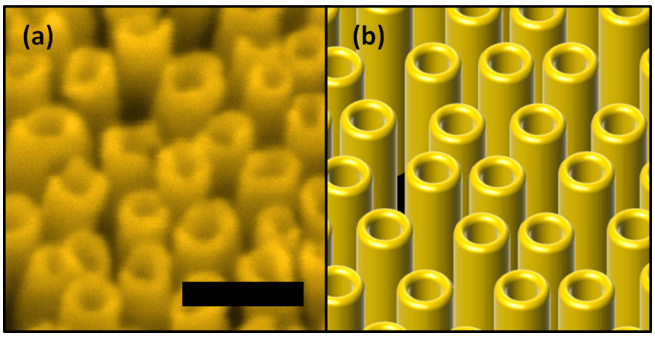

FIG. 5. (a) SEM image taken at 40° from normal of Au nanotubes (scale bar = 100 nm) and (b) matching schematic illustration.

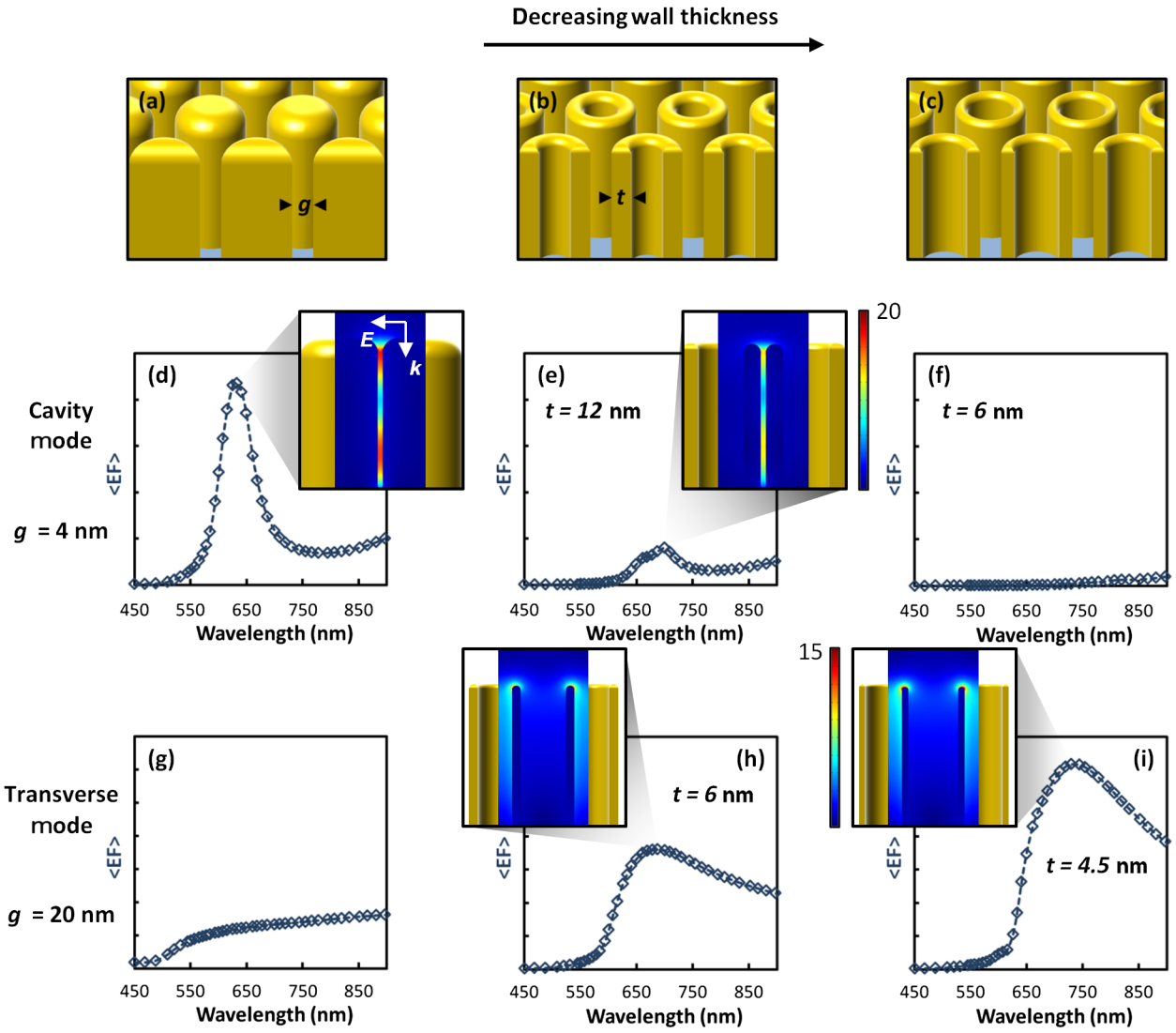

FIG. 6. Modeled data comparing the EF at normal incidence for closely spaced rods or tubes where the transverse LSPRs of neighboring structures couple into cavity modes (second row) and widely separated rods or tubes where the LSPRs have an uncoupled transverse character (third row). (a)–(c) Schematic illustration of nanorod, thick-walled-nanotube, and thin-walled-nanotube arrays showing a slice through each structure. The first set of three graphs shows the average EF for (d) nanorods and for nanotubes with (e) 12- and (f) 6-nm wall thickness, with an array period of 64 nm, inter-rod or tube spacing of 4 nm, and length 100 nm. The second set of three graphs shows the average EF for (g) nanorods and for nanotubes with (h) 6- and (i) 4.5-nm wall thickness, with an array period of 64 nm, inter-rod or tube spacing of 20 nm, and length of 100 nm. Inset: local electric field intensity profiles at resonance. (d)–(f) and (g)–(i) are plotted on the same scales, respectively.

Figs. 6(d)–6(f)]. The transverse LSPR is similarly redshifted as the wall thickness decreases (similar to the behavior of spherical nanoshells [40] and nanorings [41]). However, unlike the cavity resonance, the local fields in this case become larger, increasing the EF [as illustrated in Figs. 6(g)–6(i)]. This increase in enhancement arises because the rim of the tube focuses the local fields associated with the transverse resonance into a smaller volume at the nanotube top as the wall thickness decreases, as shown in the insets of Figs. 6(h) and 6(i). So, as we move from a nanorod array to the thick-walled-nanotube array and finally to a thin-walled-nanotube array, the character of the transverse resonance changes, becoming more near-field type due to the focusing of the fields at the rims of the tubes. As a direct result, the transverse LSPR is expected to have a much greater impact on the SERS EF.

To confirm this prediction experimentally, we fabricate the set of structures listed above: a normal Au nanorod array, an array of nanotubes with thick walls, and an array of nanotubes with thinner walls. The averaged enhancement factor $\langle EF \rangle$ and optics of these substrates are shown in Fig. 7. It is clear that the optical-extinction peak associated with the transverse resonance redshifts from approximately 520 nm for nanorods to 620 nm for

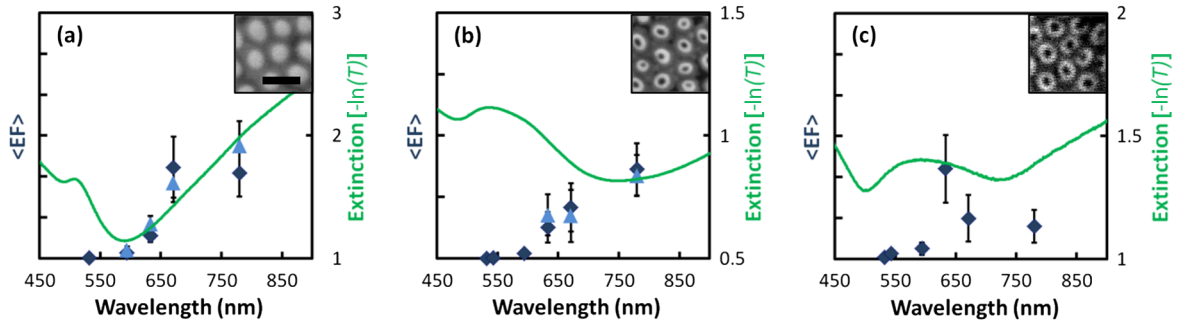

FIG. 7. Graphs comparing the measured enhancement factor ⟨EF⟩ and optical extinction $[-\ln(T)]$ at normal incidence for (a) nanorods with an average diameter of 48 nm and for (b),(c) nanotubes with average wall thickness and diameter, respectively, of 12 and 45 nm and of 9 and 50 nm. In all three cases, the average array period was 65 nm and nanorod or tube length was approximately 100 nm. The green curves indicate the optical extinction of the samples. Black-diamond and blue-triangle data points indicate the ⟨EF⟩ of the 915-cm^{-1} band of CV and the 775-cm^{-1} band of R6G, respectively. Inset: SEM images of each sample. All SEM images are on the same scale (scale bar = 100 nm).

the thinner-walled nanotubes. From the spectral profile of the EF, it is clear that, in the case of nanorods [Fig. 7(a)], the cavity resonance dominates. Similar to the substrates studied above, there is no correlation between the optics and EF, with enhancement at a maximum in the red, as is expected for nanorods of these dimensions when the cavity mode dominates the SERS response. The thick-walled tubes display a similar behavior [Fig. 7(b)], indicating that the cavity resonance still dominates SERS behavior. However, the maximum ⟨EF⟩ in this case has decreased by approximately a factor of 4. This behavior matches well with the predicted decrease of ⟨EF⟩ shown between Figs. 6(d) and 6(e). For thin-walled nanotubes, the EF generated by the cavity resonance is expected to fall dramatically, as shown in Fig. 6(f). On the other hand, the transverse LSPR of Fig. 6(i) kicks in, and with it comes a fundamental change in the spectral profile of the SERS enhancement, which is corroborated by the experimental data of Fig. 7(c). The maximum EF is no longer at 780 nm but is located at 633 nm, approximately matching the optical resonance of the transverse LSPR observed on this sample. The overall profile of the ⟨EF⟩ also much more closely matches that shown in Figs. 6(h) and 6(i). The case of the thin-walled nanotubes is the first sample to this point to show a positive correlation between the optical and SERS responses because the transverse LSPR now dominates both. The reason for this correlation is that the strongly electromagnetic-focusing thin-wall regions are uniformly present across the entire substrate, dictating not only the peak Raman response but also placing their imprint on the optical extinction. This connection for this type of substrate is strongly reiterated in the final part of the investigation.

In addition to the study of nanotube arrays in Fig. 7, we have conducted one further experimental test to confirm that the origin of SERS enhancement in this case is indeed the focused fields at the top of the tube. First, we note that, for nanorod arrays, practically no SERS enhancement is observed if the alumina template is not removed from a *nanorod* substrate [a situation illustrated in Figs. 8(a) and 8(b)], as analyte molecules cannot access the inter-rod regions where the cavity resonance generates large electric fields and thus large SERS EFs. However, for *nanotubes*, modeling indicates that fields are focused at the top of the

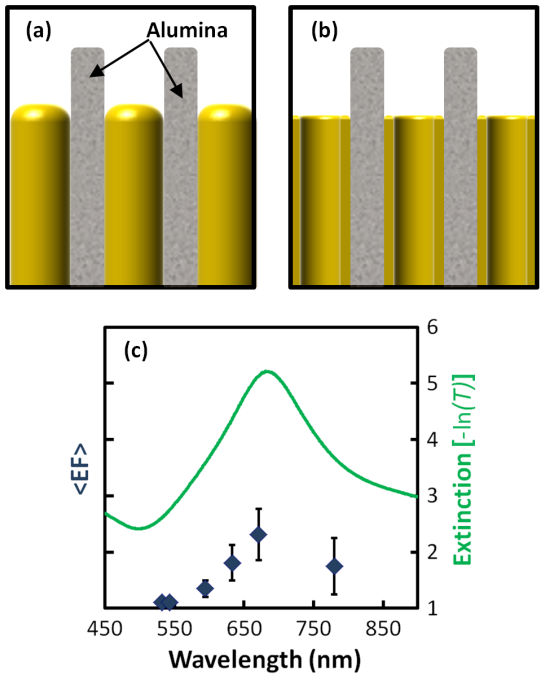

FIG. 8. Schematic illustrations of unetched gold (a) nanorod and (b) nanotube arrays still encased in the alumina template. (c) Graph showing the measured enhancement factor ⟨EF⟩ and optical extinction $[-\ln(T)]$ at normal incidence for unetched nanotubes (still encased in alumina) with average diameter of 45 nm, wall thickness of 10 nm, length of approximately 150 nm, and array period of 65 nm. The green curve indicates the optical extinction of the sample. Black-diamond data points indicate the ⟨EF⟩ of the 1617-cm^{-1} band of CV. (Signal levels for this situation were very low, and therefore this Raman band was used to reduce experimental uncertainty.)

structure (see Fig. 6), and thus an unetched nanotube structure should provide some SERS enhancement. Figure 8 shows the experimental average enhancement factor ⟨EF⟩ and optics of an unetched nanotube substrate. It is clear that, not only is significant SERS enhancement occurring, but also the peak EF matches the optical location of the transverse LSPR of the substrate well, as is expected. This result confirms not only that the transverse LSPR has a significant influence on the SERS EF in the case of nanotube arrays but also that the localized fields generating the enhancement are indeed at the tops of the tubes, as predicted by modeling. The peak of optical extinction is redshifted relative to the peak of the fully etched substrate (as in Fig. 7) due to the increased dielectric function of the surrounding material (alumina instead of air).

The series of samples described in Figs. 6 and 7 provides a particularly remarkable demonstration of the breakdown of the relationship between the near field and far field. Despite the correlation between SERS and optical responses for the final (thin-walled) sample, through the series of three samples the optical resonance progressively redshifts, while the peak SERS EF blueshifts. This opposing behavior is due to the extreme sensitivity of the local fields, and hence the SERS response, to very small changes in nanogeometry. Small changes in geometrical parameters (in this case, the wall thickness) can drastically alter the character of the LSPRs, changing their character from far-field type to near-field type and vice versa, hence significantly changing the near-field patterns associated with them, and even completely changing which LSPR dominates the SERS response, resulting in such surprising behavior. So, not only can near-field and far-field properties be tuned almost independently (as demonstrated in Sec. III B), in some cases they behave oppositely, reinforcing the point that the relationship between these two related behaviors is often not a simple one.

V. SUMMARY AND CONCLUSIONS

In summary, we have demonstrated the importance of identifying the far-field-type or near-field-type character of particular LSPRs in determining their influence on the behavior of a surface. We have shown that near-field-type resonances can dominate the SERS response of a substrate while having essentially no optical signature, and contrariwise that far-field-type resonances can dominate the optical response while having no major impact on SERS. Thus, the optical resonances of a substrate can be a very poor indicator of SERS performance. As a result, for "real" substrates with multiple LSPRs, it is possible to tune far-field and near-field properties almost independently. Furthermore, it has been shown that a detailed understanding of which particular LPSRs dominate SERS and how they behave (as obtained through modeling) can allow us to accurately predict the behavior of substrates that exhibit multiple LPSRs without relying on often misleading optical measurements. Finally, we have demonstrated that the changes in nanogeometry or the interaction between neighboring particles that are used to tune the wavelength of an LSPR can also have a profound impact on its character, changing its behavior from far-field type to near-field type or vice versa. These changes can alter the relationship between the SERS and optical signatures of a substrate, so that the tuning of far-field properties will not necessarily affect the near field in the same way. The physical principles demonstrated here should help inform the design of future SERS substrates, in particular, the design of routine substrates tailored to a specific excitation wavelength. These conclusions should also be of significant interest in any plasmonic application in which the interaction between the far field and near field is of central importance.

ACKNOWLEDGMENTS

A. M. and R. J. P. acknowledge support from EPSRC Grant No. EP/H000917/1 ("Active Plasmonics"), and P. D. likewise acknowledges funding from the EC Grant "BONAS" (Project No. 261685). M. D. D. is grateful to the Department of Education and Learning and Queen's University Belfast.

[1] S. Lal, S. Link, and N. J. Halas, *Nano-optics from Sensing to Waveguiding*, Nat. Photonics **1**, 641 (2007).
[2] K. A. Willets and R. P. Van Duyne, *Localized Surface Plasmon Resonance Spectroscopy and Sensing*, Annu. Rev. Phys. Chem. **58**, 267 (2007).
[3] K. L. Kelly, E. Coronado, L. L. Zhao, and G. C. Schatz, *The Optical Properties of Metal Nanoparticles: The Influence of Size, Shape, and Dielectric Environment*, J. Phys. Chem. B **107**, 668 (2003).
[4] S. Link and M. A. El-Sayed, *Spectral Properties and Relaxation Dynamics of Surface Plasmon Electronic Oscillations in Gold and Silver Nanodots and Nanorods*, J. Phys. Chem. B **103**, 8410 (1999).
[5] J. A. Schuller, E. S. Barnard, W. Cai, Y. C. Jun, J. S. White, and M. L. Brongersma, *Plasmonics for Extreme Light Concentration and Manipulation*, Nat. Mater. **9**, 193 (2010).
[6] E. C. Le Ru and P. G. Etchegoin, *Principles of Surface-Enhanced Raman Spectroscopy* (Elsevier, Amsterdam, 2009).
[7] P. L. Stiles, J. A. Dieringer, N. C. Shah, and R. R. Van Duyne, *Surface-Enhanced Raman Spectroscopy*, Annu. Rev. Anal. Chem. **1**, 601 (2008).
[8] P. Evans, W. R. Hendren, R. Atkinson, G. A. Wurtz, W. Dickson, A. V. Zayats, and R. J. Pollard, *Growth and Properties of Gold and Nickel Nanorods in Thin Film Alumina*, Nanotechnology **17**, 5746 (2006).
[9] W. R. Hendren, A. Murphy, P. Evans, D. O'Connor, G. A. Wurtz, A. V. Zayats, R. Atkinson, and R. J. Pollard, *Fabrication and Optical Properties of Gold Nanotube Arrays*, J. Phys. Condens. Matter **20**, 362203 (2008).

[10] A. Murphy, J. McPhillips, W. Hendren, C. McClatchey, R. Atkinson, G. Wurtz, A. V. Zayats, and R. J. Pollard, *The Controlled Fabrication and Geometry Tunable Optics of Gold Nanotube Arrays*, Nanotechnology **22**, 045705 (2011).

[11] E. Le Ru and P. Etchegoin, *Rigorous Justification of the $|E|^4$ Enhancement Factor in Surface Enhanced Raman Spectroscopy*, Chem. Phys. Lett. **423**, 63 (2006).

[12] E. C. Le Ru, E. Blackie, M. Meyer, and P. G. Etchegoin, *Surface Enhanced Raman Scattering Enhancement Factors: A Comprehensive Study*, J. Phys. Chem. C **111**, 13794 (2007).

[13] P. G. Etchegoin and E. C. Le Ru, *A Perspective on Single Molecule SERS: Current Status and Future Challenges*, Phys. Chem. Chem. Phys. **10**, 6079 (2008).

[14] E. Le Ru, M. Meyer, and P. Etchegoin, *Proof of Single-Molecule Sensitivity in Surface Enhanced Raman Scattering (SERS) by Means of a Two-Analyte Technique*, J. Phys. Chem. B **110**, 1944 (2006).

[15] J. Theiss, P. Pavaskar, P. M. Echternach, R. E. Muller, and S. B. Cronin, *Plasmonic Nanoparticle Arrays with Nanometer Separation for High-Performance SERS Substrates*, Nano Lett. **10**, 2749 (2010).

[16] M. J. Banholzer, J. E. Millstone, L. Qin, and C. A. Mirkin, *Rationally Designed Nanostructures for Surface-Enhanced Raman Spectroscopy*, Chem. Soc. Rev. **37**, 885 (2008).

[17] X. Zhang, J. Zhao, A. V. Whitney, J. W. Elam, and R. P. Van Duyne, *Ultrastable Substrates for Surface-Enhanced Raman Spectroscopy: Al_2O_3 Overlayers Fabricated by Atomic Layer Deposition Yield Improved Anthrax Biomarker Detection*, J. Am. Chem. Soc. **128**, 10304 (2006).

[18] A. D. McFarland, M. A. Young, J. A. Dieringer, and R. P. Van Duyne, *Wavelength-Scanned Surface-Enhanced Raman Excitation Spectroscopy*, J. Phys. Chem. B **109**, 11279 (2005).

[19] N. Felidj, J. Aubard, G. Levi, J. R. Krenn, A. Hohenau, G. Schider, A. Leitner, and F. R. Aussenegg, *Optimized Surface-Enhanced Raman Scattering on Gold Nanoparticle Arrays*, Appl. Phys. Lett. **82**, 3095 (2003).

[20] E. C. Le Ru, C. Galloway, and P. G. Etchegoin, *On the Connection between Optical Absorption/Extinction and SERS Enhancements*, Phys. Chem. Chem. Phys. **8**, 3083 (2006).

[21] A. M. Michaels, M. Nirmal, and L. Brus, *Surface Enhanced Raman Spectroscopy of Individual Rhodamine 6G Molecules on Large Ag Nanocrystals*, J. Am. Chem. Soc. **121**, 9932 (1999).

[22] L. L. Tay, J. Hulse, D. Kennedy, and J. P. Pezacki, *Surface-Enhanced Raman and Resonant Rayleigh Scatterings from Adsorbate Saturated Nanoparticles*, J. Phys. Chem. C **114**, 7356 (2010).

[23] M. I. Stockman, V. M. Shalaev, M. Moskovits, R. Botet, and T. F. George, *Enhanced Raman Scattering by Fractal Clusters: Scale-Invariant Theory*, Phys. Rev. B **46**, 2821 (1992).

[24] V. Markel, V. Shalaev, P. Zhang, W. Huynh, L. Tay, T. Haslett, and M. Moskovits, *Near-Field Optical Spectroscopy of Individual Surface-Plasmon Modes in Colloid Clusters*, Phys. Rev. B **59**, 10903 (1999).

[25] P. Zhang, T. L. Haslett, C. Douketis, and M. Moskovits, *Mode Localization in Self-Affine Fractal Interfaces Observed by Near-Field Microscopy*, Phys. Rev. B **57**, 15513 (1998).

[26] Y. Fang, N. Seong, and D. D. Dlott, *Measurement of the Distribution of Site Enhancements in Surface-Enhanced Raman Scattering*, Science **321**, 388 (2008).

[27] J. M. McMahon, S. Li, L. K. Ausman, and G. C. Schatz, *Modeling the Effect of Small Gaps in Surface-Enhanced Raman Spectroscopy*, J. Phys. Chem. C **116**, 1627 (2011).

[28] K. L. Wustholz, A. I. Henry, J. M. McMahon, R. G. Freeman, N. Valley, M. E. Piotti, M. J. Natan, G. C. Schatz, and R. P. V. Duyne, *Structure-Activity Relationships in Gold Nanoparticle Dimers and Trimers for Surface-Enhanced Raman Spectroscopy*, J. Am. Chem. Soc. **132**, 10903 (2010).

[29] D. P. Lyvers, J. Moon, A. V. Kildishev, V. M. Shalaev, and A. Wei, *Gold Nanorod Arrays as Plasmonic Cavity Resonators*, ACS Nano **2**, 2569 (2008).

[30] M. Bora, B. J. Fasenfest, E. M. Behymer, A. S. Chang, H. T. Nguyen, J. A. Britten, C. C. Larson, J. W. Chan, R. R. Miles, and T. C. Bond, *Plasmon Resonant Cavities in Vertical Nanowire Arrays*, Nano Lett. **10**, 2832 (2010).

[31] H. A. Atwater and A. Polman, *Plasmonics for Improved Photovoltaic Devices*, Nat. Mater. **9**, 205 (2010).

[32] S. Link, M. Mohamed, and M. El-Sayed, *Simulation of the Optical Absorption Spectra of Gold Nanorods as a Function of Their Aspect Ratio and the Effect of the Medium Dielectric Constant*, J. Phys. Chem. B **103**, 3073 (1999).

[33] C. F. Bohren and D. R. Huffman, *Absorption and Scattering of Light by Small Particles* (Wiley, New York, 1998).

[34] P. K. Jain and M. A. El-Sayed, *Plasmonic Coupling in Noble Metal Nanostructures*, Chem. Phys. Lett. **487**, 153 (2010).

[35] R. Kullock, S. Grafstroem, P. R. Evans, R. J. Pollard, and L. M. Eng, *Metallic Nanorod Arrays: Negative Refraction and Optical Properties Explained by Retarded Dipolar Interactions*, J. Opt. Soc. Am. B **27**, 1819 (2010).

[36] M. D. Doherty, A. Murphy, J. McPhillips, R. J. Pollard, and P. Dawson, *Wavelength Dependence of Raman Enhancement from Gold Nanorod Arrays: Quantitative Experiment and Modeling of a Hot Spot Dominated System*, J. Phys. Chem. C **114**, 19913 (2010).

[37] X. Deng, G. B. Braun, S. Liu, P. F. Sciortino, Jr., B. Koefer, T. Tombler, and M. Moskovits, *Single-Order, Subwavelength Resonant Nanograting as a Uniformly Hot Substrate for Surface-Enhanced Raman Spectroscopy*, Nano Lett. **10**, 1780 (2010).

[38] A. Gopinath, S. V. Boriskina, W. R. Premasiri, L. Ziegler, B. M. Reinhard, and L. Dal Negro, *Plasmonic Nanogalaxies: Multiscale Aperiodic Arrays for Surface-Enhanced Raman Sensing*, Nano Lett. **9**, 3922 (2009).

[39] C. Haynes and R. Van Duyne, *Plasmon-Sampled Surface-Enhanced Raman Excitation Spectroscopy*, J. Phys. Chem. B **107**, 7426 (2003).

[40] S. Oldenburg, J. Jackson, S. Westcott, and N. Halas, *Infrared Extinction Properties of Gold Nanoshells*, Appl. Phys. Lett. **75**, 2897 (1999).

[41] J. Aizpurua, P. Hanarp, D. Sutherland, M. Kall, G. Bryant, and F. de Abajo, *Optical Properties of Gold Nanorings*, Phys. Rev. Lett. **90**, 057401 (2003).